nature food

Article

https://doi.org/10.1038/s43016-023-00817-7

Dual-sensory fusion self-powered triboelectric taste-sensing system towards effective and low-cost liquid identification

Received: 21 December 2022

Accepted: 10 July 2023

Published online: 10 August 2023

Check for updates

Xuelian Wei[1,2], Baocheng Wang[1,2], Xiaole Cao[1,2], Hanlin Zhou[1], Zhiyi Wu[1,2] ✉ & Zhong Lin Wang[1,3,4] ✉

Infusing human taste perception into smart sensing devices to mimic the processing ability of gustatory organs to perceive liquid substances remains challenging. Here we developed a self-powered droplet-tasting sensor system based on the dynamic morphological changes of droplets and liquid–solid contact electrification. The sensor system has achieved accuracies of liquid recognition higher than 90% in five different applications by combining triboelectric fingerprint signals and deep learning. Furthermore, an image sensor is integrated to extract the visual features of liquids, and the recognition capability of the liquid-sensing system is improved to up to 96.0%. The design of this dual-sensory fusion self-powered liquid-sensing system, along with the droplet-tasting sensor that can autonomously generate triboelectric signals, provides a promising technological approach for the development of effective and low-cost liquid sensing for liquid food safety identification and management.

The research on taste sensing is important to the development of the food industry, food safety and the innovation of food technology. In particular, taste in sensory functions plays a prominent role in the identification and analysis of liquid food types. The concept of a bionic electronic tongue was first proposed in a study[1] in 2005, in which sensor arrays were used to simulate human taste buds for detecting the taste of liquid samples. With advances in robotic taste-sensing system research, the application of electronic tongue technology is becoming increasingly extensive. Among these advances, the chemical sensor is the most common method at present. IBM Research has developed a chemical taste perception tool, Hypertaste, which uses electrochemical sensors to quickly and reliably identify different types of liquid[2]. A study[3] explored the perceived umami intensity in food matrices through chemical analysis and an electronic tongue to provide options for food industries to select the proper method for evaluating the perceived umami intensity of various foods. Researchers at the University of Cambridge have proposed a robotic set-up that can train chef robots to taste the saltiness of food, generating visualized taste images[4]. In addition, electronic tongues or taste sensors have also been applied to the wine industry[5], pharmaceutical applications[6] and the dairy industry[7]. Electronic tongues can also handle what people would not or could not taste. However, the implementation of an electronic taste requires costly and complex analysis, and the uncertainty of 'tasting' makes it difficult for robotic automation. Meanwhile, for the chemical-sensing method, because of the selective recognition of sensor units and the cross-reaction interaction of sensor arrays, there is a single matching problem between the sensor unit and the test object. Regarding energy supply in the design of smart sensors, it is inconvenient to frequently charge or replace batteries[8,9]. Therefore, it is necessary to develop intelligent taste sensors that can actively generate electrical signals.

Triboelectric sensors with high sensitivity, fast response, light weight and low cost are generally designed to monitor small mechanical electrical signals in self-powered mode[10]. Previous research has made fruitful efforts in promoting the intelligent 'five senses' with the assistance of

[1]Beijing Institute of Nanoenergy and Nanosystems, Chinese Academy of Sciences, Beijing, P. R. China. [2]School of Nanoscience and Engineering, University of Chinese Academy of Sciences, Beijing, P. R. China. [3]Georgia Institute of Technology, Atlanta, GA, USA. [4]Yonsei Frontier Lab, Yonsei University, Seoul, Republic of Korea. ✉e-mail: wuzhiyi@binn.cas.cn; zhong.wang@mse.gatech.edu

triboelectric nanogenerators (TENGs; electron transfer is generated by friction between different materials in TENGs). Friction is capable of generating not only heat but also smell. A closed-loop wearable system based on the principle of TENGs and olfactory receptors has been proposed to recognize different gas molecules[11]. A self-powered triboelectric auditory sensor for social robots has been designed[12]. An ion-doped gelatin-hydrogel-based touch sensor has been developed to identify not only contact with an object but also deformation force[13]. Studies[14,15] have developed tactile sensing in intelligent robots. In addition, taste perception always subconsciously combines multiple senses, which objectively creates the possibility of simultaneous recognition about the same food from different angles. For the analysis of liquid, it is more accurate to use both taste and sight than to use one of these senses alone.

Here we present a droplet-based triboelectric taste-sensing system that integrates two taste-sensing units into a taste sensor and outputs a series of triboelectric signals. Combined with deep-learning data analytics, a 'liquid fingerprint database' can be established to implement the preliminary identification of different liquids, and a high accuracy of 91.3% is achieved in the robot taste application. Furthermore, the visual information of different droplets is fused with the sensing signal information to further extract the complete visual characteristics of liquids. Thus, a more comprehensive liquid recognition function can be achieved with the assistance of image recognition. We include liquid visual information that further facilitates the perception capability of the taste-sensing system, and the recognition accuracy is up to 96.0%. This dual-sensory fusion self-powered liquid-sensing system, along with the sensing principle and design of the triboelectric droplet-tasting sensor (TDTS) provides an effective and low-cost way of evaluating liquid food flavour, detecting sugar, monitoring the environment and testing alcohol content, without any external power supply. The intelligent liquid-sensing system has the potential to improve the efficiency of food monitoring and expand the scope of food control and has a great pushing effect for the food safety management system as an effective means in the rapid detection of liquid food.

Results

Intelligent triboelectric taste-sensing system

The human taste recognition system is a highly complex perceptual mechanism, and the tongue is the main organ of taste, with thousands of taste receptors (taste buds). Taste buds perform the task of signal recognition and signal processing to complete the process of taste perception[16,17] (Fig. 1a). Inspired by the multisensory interaction of the taste system, we designed a deep-learning-network-assisted, intelligent droplet-based taste-sensing system that includes a TDTS and an image sensor (Fig. 1b,c). The TDTS consists of two well-designed, single-electrode-mode TENGs with independent copper electrodes, and has the advantage of actively generating triboelectric signals without the need for an external power supply. Feature extraction is an important and critical part of realizing the recognition function of the intelligent droplet-based taste-sensing system. Specifically, the characteristic extraction of liquids in our experiment comes not only from the double triboelectric signals generated by droplets triggering the two copper electrodes but also from the photographic images of the droplets captured by the image sensor. This technique is bound to extract more complete feature information of liquids, thus achieving a more accurate and comprehensive liquid identification.

Mechanism and parameters of the sensor with one electrode

Inspired by the dynamic morphological changes of a water droplet sliding down an inclined surface (Supplementary Video 1) and the phenomenon of the droplet in contact with a solid object generating a triboelectric signal[18], we are developing a simple droplet-based TENG for efficient liquid sensing by probing the difference in charge transfer between liquid and solid surfaces. To concisely and intuitively demonstrate the feasibility of this liquid-sensing strategy, a droplet TENG with one spatially arranged metallic electrode is fabricated. Polymer films with a certain hydrophobicity are considered as contact materials so that droplets can easily slip off the inclined surface adhered to a polymer film. Figure 2a shows the charge transfer between the water droplet and the polymer. When the water droplet falls and makes contact with the polymer surface, the polymer will be negatively charged at the contact interface, and the water droplet will be positively charged according to the electrical double layer theory (Fig. 2a(i)). The charges on the water droplet then continue to accumulate during the subsequent sliding process on the polymer surface. When the water droplet slides to the copper electrode position, the excess charge on the water droplet leads to the induced charge on the copper electrode (Fig. 2a(ii)), while the excess charge on the polymer film surface leads to another induced charge after the water droplet moves away from the electrode position (Fig. 2a(iii)). Finally, the charges on the water droplet accumulate until the water droplet drops off the incline (Fig. 2a(iv)). Figure 2b shows the morphological changes (Fig. 2b, top and middle, and Supplementary Video 2) and the simulation results of the liquid volume fraction changes (Figure 2b, bottom, and Supplementary Video 3) of a droplet sliding down an incline at different moments. Simultaneously, the velocity field simulation of a sliding water droplet is also shown to better observe the morphological changes of the droplets (Supplementary Fig. 1 and Supplementary Video 4).

All the droplets are released from the grounded stainless steel needle of a microsyringe pump (50 µl per drop) at a preset velocity, and the initial droplet height is fixed at 0.8 cm. During the contact process of water droplets with the polymer surface, the morphology of the droplet undergoes a dynamic alternation of spreading, contracting and respreading until the droplet falls. The differences in electron affinity and physicochemical properties of different liquids allow the charge transfer triggered at electrodes to form different triboelectric signals, which can then be used as probes for liquid sensing. Considering the charge saturation effect, we always apply the first droplet in our experiments. A series of parameters, such as polymer material, droplet type, droplet falling angle, initial velocity, droplet volume and electrode width, will affect the subsequent design of the droplet-tasting sensor, so it is necessary to conduct further exploration. We quantify the parameters by the charge transfer between the polymer film and the droplet. Figure 2c shows the output current of deionized (DI) water droplets in contact with different triboelectric layer materials. The 30 µm fluorinated ethylene propylene (FEP) has the highest output current, which is inseparable from its good electron affinity and high contact angle (Supplementary Fig. 2). Figure 2d compares the output current of different electrode widths at different droplet falling angles (45°, 50°, 55° and 60°; Supplementary Fig. 3). Compared with other sizes, the highest output current is always obtained for an electrode width of 1 cm at the same falling angle, which should be influenced by a combination of the charge saturation effect and the time required for the charge-transfer process between the droplet and the polymer film interface. However, the relationship between the droplet falling angle and the output current is relatively complicated (Fig. 2f). In addition to the moving velocity of the droplet on the inclined plane, the falling angle also affects the contact area between the droplet and the polymer film, the interaction time between the droplet and the sensing electrode, and the dropping point of the droplet on the polymer surface. These parameters have different response trends after being affected by the falling angle, which jointly act on the output current. A more detailed discussion is shown in Supplementary Note 1. Therefore, the falling angle is incorporated as a variable for the sensor structure parameters. Meanwhile, the charge transfer of five different kinds of droplets sliding on the FEP film is studied (electrode width of 1 cm). The amount of charge transfer and the currents for different droplets show distinct differences (Fig. 2e). These results sufficiently show that the triboelectric signal information can be used as a fingerprint of liquids for identification. In addition, for a small falling angle (45°), both the initial velocity

 https://doi.org/10.1038/s43016-023-00817-7

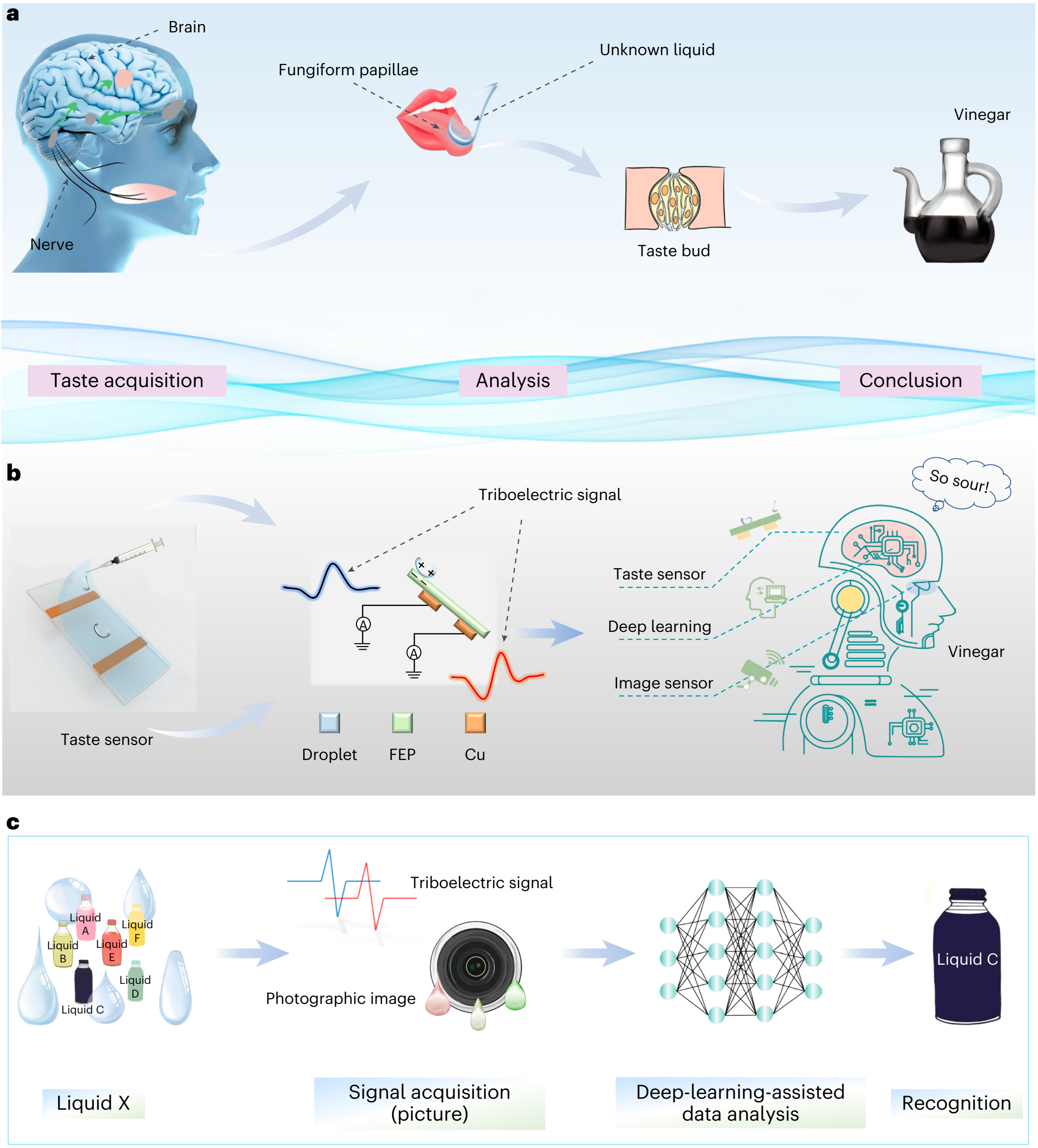

Fig. 1 | Droplet-based triboelectric taste-sensing system mimicking the human taste receptor. a, Schematic diagram of human taste formation. Food stimulates taste receptors (taste buds) and information is transmitted through the nerves to the taste centre of the brain, which is finally analysed by the brain to form the sense of taste. **b**,**c**, The intelligent taste-sensing system (**b**) and its recognition process (**c**) that relies on triboelectric signals and liquid images for more accurate taste perception with the assistance of deep learning.

and the droplet volume show a positive relationship with the output current. The current increases with the initial velocity or the droplet volume (Fig. 2g,h). The above presentation provides preparation for further development of this triboelectric-based droplet-tasting sensor.

Mechanism and sensing characteristics of the TDTS

Taste buds on our tongue help people perceive flavours, and each taste bud contains taste cells that can discriminate between different tastes (Fig. 3a)[19]. Although it is not possible to completely simulate the perception mechanism of the human gustatory system, the basic recognition mechanism can be achieved by feedback electrical signals obtained through the differences in some major physicochemical properties of liquids. Increasing the number of electrodes can obtain more electrical signals, so that droplets can better respond to changes of the dynamic morphology and output more characteristic information. To increase the accuracy of taste sensors, we design a droplet-tasting sensor with two spatially arranged electrodes, and the two sets of triboelectric signals generated will certainly identify more characteristics of liquids. The working mechanism of the TDTS is described, as shown in Fig. 3b. A schematic diagram of one electrode and two electrodes is shown in Supplementary Fig. 4. A droplet sliding over electrode 1 has been described previously (Fig. 2a). This is similar to the droplet sliding over electrode 2 and charges on the droplet continue to accumulate. Then, when the droplet separates from the bottom of the polymer, the metal electrode loses electrons to the ground to shield static charges on the polymer surface.

The distance between the two electrodes is investigated as an optimization parameter in Fig. 3c and Supplementary Fig. 5. Here, I_1 and

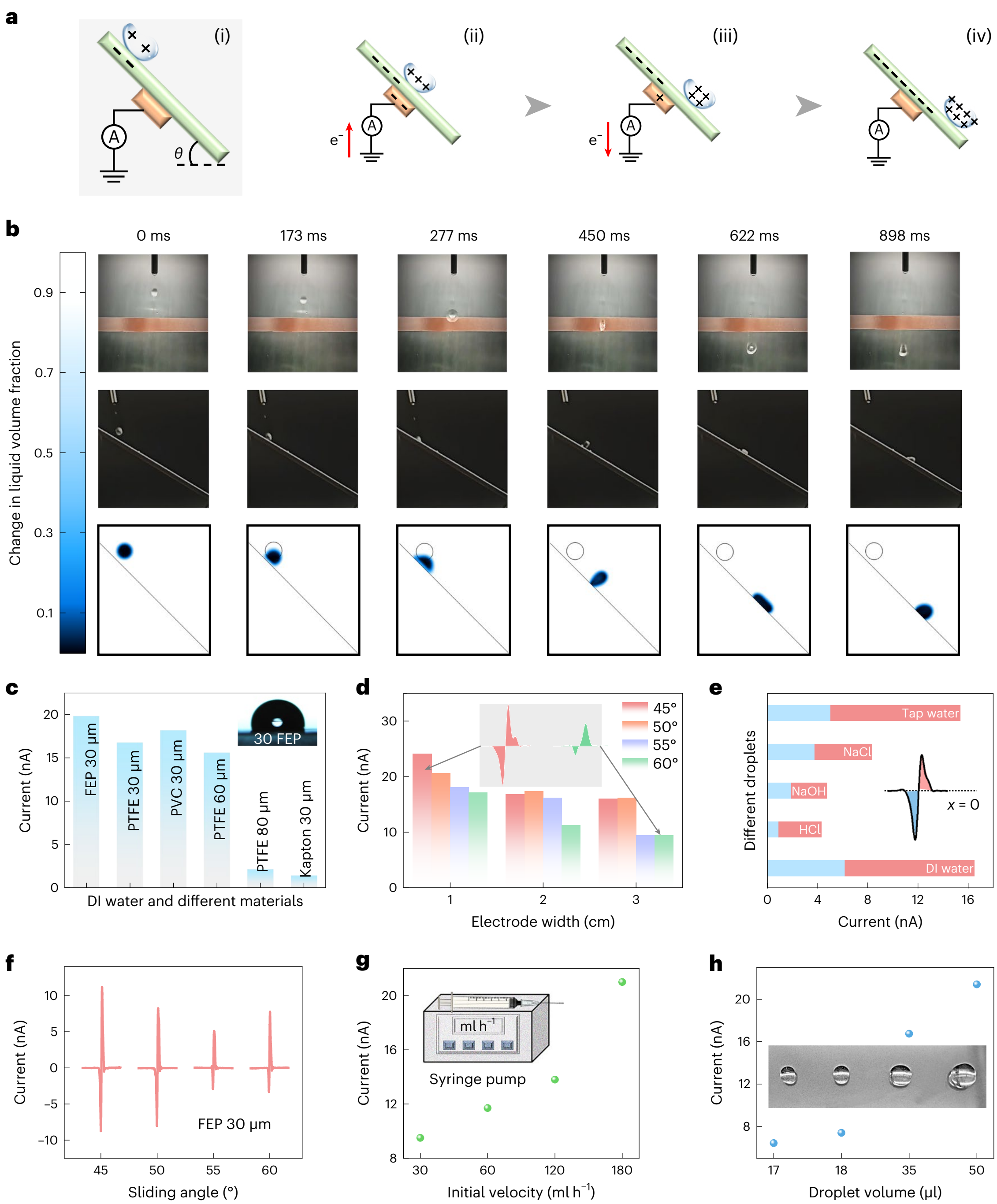

Fig. 2 | The working principle of a droplet-tasting sensor with one spatially arranged electrode, the sliding process of a water droplet and the electrical output of a single-electrode droplet-tasting sensor. a, Step-by-step principle of the droplet-tasting sensor with a single electrode. **b**, A series of pictures detail the dynamic sliding motion of one water droplet. The time represents the different moments at which a droplet slides down an inclined plane. The colour scale of the heat map (blue) represents the change in liquid volume fraction. The droplet height is set at 0.8 cm. **c**, Output current of a water droplet contacted and separated with different materials. The type and thickness of polymer films used are indicated on the chart. The inset shows the contact angle of the DI water on the surface of 30-μm-thick FEP. **d**, Output current of single-electrode taste sensors with different electrode widths slipping at various angles (DI water, 30 μm FEP and the initial velocity of the droplet is set to 60 ml h^{-1}). The inset shows the red curve (electrode width, 1 cm; falling angle, 45°) and the green curve (electrode width, 3 cm; falling angle, 60°). **e**, Output current of the 30 μm FEP with different droplets: tap water, NaCl solution (0.5 M), NaOH solution (pH 13), HCl solution (pH 3) and DI water. The red zone represents the forward current, and the blue zone indicates the reverse current. *x* represents the horizontal axis in an orthogonal plane coordinate system. **f**, Output current of a water droplet sliding through the sensor placed at different angles (30 μm FEP, 1 cm electrode width). **g**,**h**, Effect of initial velocity (**g**) and droplet volume (**h**) on output signal. PVC, polyvinyl chloride.

I_2 denote the transferred charges per unit time for electrode 1 and electrode 2, respectively. Therefore, the transferred charges between the two electrodes per unit time can be calculated from $I_1 - I_2$. The effect of the electrode distance on the output current is still relatively obvious, regardless of the falling angle. However, when the electrode distance is 4 cm, the output current is higher than that of other distances (Fig. 3d). In addition, the output current of electrode 1 and electrode 2 always increases with the initial velocity (the falling angle is 50° or 60°; Fig. 3e).

https://doi.org/10.1038/s43016-023-00817-7

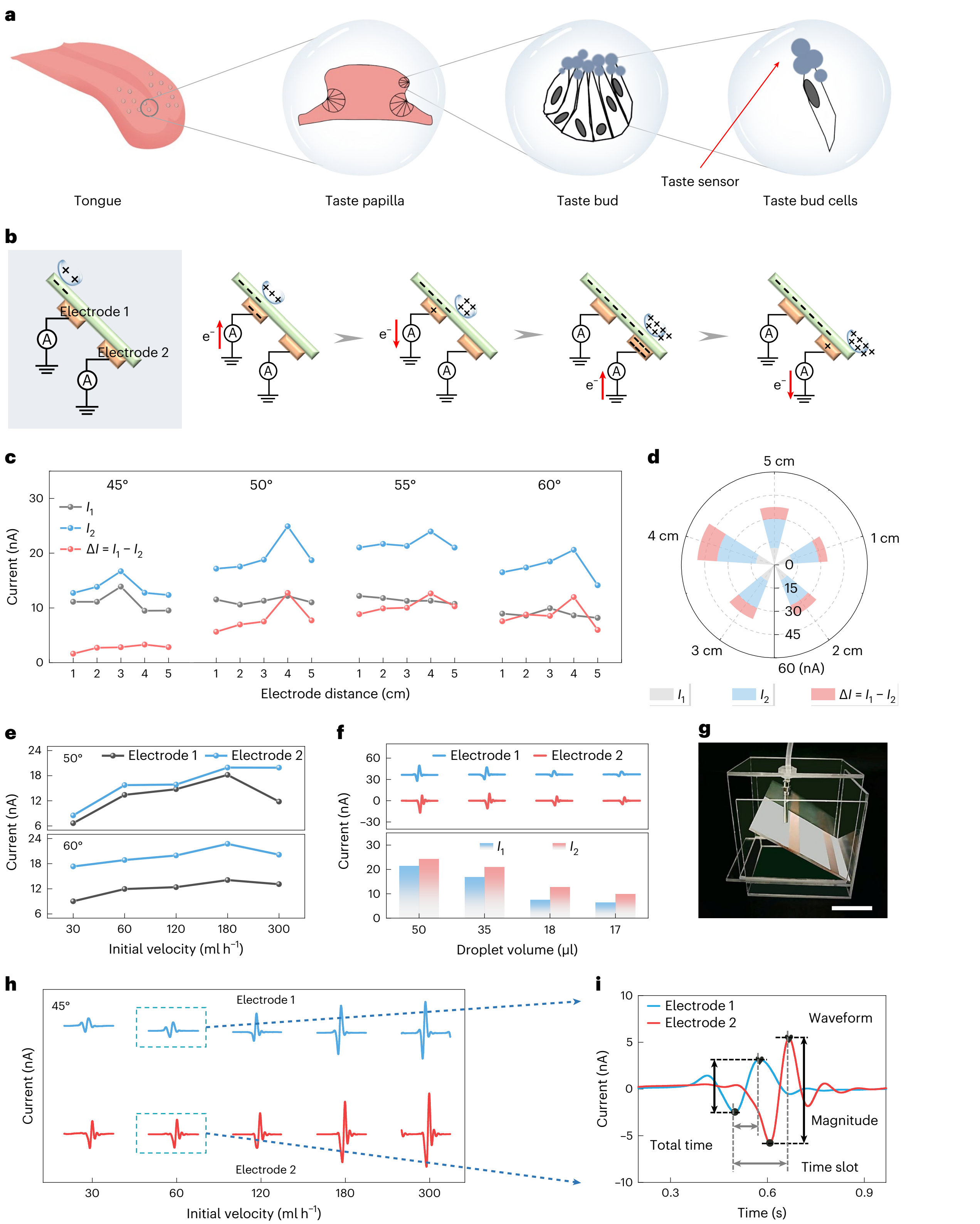

Fig. 3 | Mechanism and sensing characteristics of a TDTS for sensing a droplet at two electrodes. a, The structure of the taste buds distributed on the human tongue. **b**, Schematic diagram of the TDTS. **c**, Relationship between the electrode distance and the output current of the TDTS under different sliding angles. I_1 and I_2 represent the transferred charges per unit time for electrode 1 and electrode 2, respectively. **d**, Comprehensive selection rules of electrode distances for the TDTS. **e**,**f**, Initial velocity (**e**) and droplet volume (**f**) versus output signals from electrode 1 and electrode 2. **g**, Photograph of a TDTS. Scale bar, 4 cm. **h**, The typical current signal profile of the TDTS on electrode 1 and electrode 2 when a droplet separated from the FEP film adhered to two copper electrodes. **h**, The current response of the two electrodes. **i**, Zoomed-in view of **h** for analysing the current response of the two electrodes to a droplet. Waveform refers to the complete waveform of the identified liquids corresponding to two current signals. Magnitude refers to the magnitude of the currents. Total time represents the total time taken to complete the waveforms of liquids. Time slot represents the interval time of the valley to the peak.

https://doi.org/10.1038/s43016-023-00817-7

The results at 300 ml h^{-1} are different, from which we can infer that, at a large falling angle, the output current is no longer only affected by the initial velocity of the droplet but is also related to the contact area between the droplet and the polymer film, the interaction time between them, the impact position of the droplet on the polymer surface and other parameters (Supplementary Note 1).

Figure 3f shows the relationship between droplet volume and output current. We used different types of needle to control the droplet size during the experiment. A larger droplet volume brings a larger charge transfer, which changes the current amplitude, but the trend of the waveform remains consistent. Figure 3g demonstrates the structure of the TDTS with an external acrylic shell; this simple and open structure enhances the possibility of practical applications. Considering an angle of 45°, a pair of current signals with different initial velocities of droplets are shown in Fig. 3h, which indicates not only that the amplitude of output currents increases with the velocity when the falling angle is small but also that some obvious characteristics can be observed from the larger version of the waveforms (Fig. 3i). For example, the magnitudes of the forward and reverse current signals, the time slot between the peak–valley of a waveform and the time slot between the peak–peak of two waveforms can be seen. All these features can be extracted individually as effective information in preparation for liquid identification.

Triboelectric signal characteristics of different liquids

Based on the above working principle of the TDTS, to further demonstrate the effectiveness and versatile sensing capability of this liquid sensor, the current response from a wider range of liquids, including 14 different groups of liquids, is tested and enumerated to fully illustrate the characteristics of multiple liquids (Fig. 4a). The blue curve represents the induced current signal generated by the induced electrode 1, and the red curve corresponds to electrode 2. For comparison, the test fluid also contains both drinking water and tap water. The current magnitude is an obvious characteristic, which is mainly attributed to the differences in the ability of different liquids to gain or lose electrons and the concentration of liquid ions. An increased concentration of ions can lead to a suppression in the amount of transferred charge, just as a salt solution results in a significant reduction of the electric output[20]. Accordingly, compared with white vinegar, drinking water has a greater current output due to smaller free ions[21] (the current magnitudes of electrode 1 (h_1) and electrode 2 (h_2) of drinking water are higher than those of white vinegar; Fig. 4a, top left inset).

In addition, the affinity of various aqueous solutions to the polymer film (30 μm FEP) also affects the output electrical signal. Low concentrations of monosodium glutamate (MSG) water and sugar water show poor affinity for the FEP film, with less liquid residue during the sliding process. As a consequence, the overall current output is mainly determined by the triboelectric signal of water. In contrast, liquor and black coffee suspensions more easily adsorb on the surface of FEP than water and have more surface residue during sliding, which is more likely to result in lower output performance[22]. Supplementary Video 5 shows the triboelectric signal triggered by a coffee droplet sliding on the surface of the FEP film. It can be seen clearly that the coffee droplet slides in a strand shape (Supplementary Fig. 6d–f), which is directly related to its viscosity. Throughout the process of the coffee droplet touching and sliding across electrode 1, the coffee flow (strand) does not immediately induce triboelectric signals on the program interface. When the front end of the coffee flow just touches electrode 2, the electrical curves of the two channels begin to appear. As the coffee flow slowly slides on the polymer surface, the triboelectric signals in channel 1 and channel 2 change simultaneously, after which the two signal waveforms tend to be complete synchronously (the triboelectric signals generated by the black coffee droplet almost coincide in Fig. 4a). We also show the triboelectric signal triggered by a water droplet sliding on the surface of the FEP film (Supplementary Video 6). When the water droplet first contacts electrode 1, a triboelectric signal from channel 1 begins to arise. As the water droplet gradually slides to the central position of electrode 1, the output current curve of channel 1 builds up to a peak, indicating that the amount of transferred charge between the droplet and the polymer film tends to be saturated. Subsequently, the water droplet continues to slide, and there is no waveform in channel 2 at this stage. As the water droplet slides to the position of electrode 2, a triboelectric signal starts to appear in channel 2, and the waveform of channel 1 is gradually complete. Similarly to the sliding seen over electrode 1, the output current curve of channel 2 shows a peak as the water droplet slides to the centre of electrode 2. After that, the waveforms of both channels are gradually complete as the water droplet continues to flow.

In addition, the current waveform (Fig. 4a, top right inset), the total time of sliding (Fig. 4a, bottom left inset) and the valley-to-peak time slot (Fig. 4a, bottom right inset) are also disturbed. The total time taken to complete the waveforms of all liquids is summarized in Fig. 4b, where the graph shows the trend of the total time of all measured liquids more intuitively. Supplementary Figs. 7 and 8 show the data for time slot 1 and time slot 2, respectively (where time slot 1 represents the interval time of the valley to the peak in response to electrode 1 and time slot 2 represents the interval time between the valley of electrode 1 and the peak of electrode 2). These results further enhance the signal differentiation between different liquids.

Figure 4c and Supplementary Fig. 9 show the viscosity of several liquids. The viscosity of a fluid directly affects its fluidity. The viscosity of both black coffee suspension and liquor is higher than that of other fluids, meaning less fluidity. The experimental results also confirm the above conclusion. Furthermore, the pH value of the droplet also influences the output performance. Droplets with different pH values in our experiment are aqueous solutions containing a certain concentration of HCl and NaOH. This charge-transfer process and the amount of charge transferred are related to the 'screen effect' of free ions[23,24]. The change in liquid composition will cause a corresponding change in the output current signal. If more comprehensively quantified, this type of variation can provide an ideal sensing ability as a 'dual characteristic' of liquid for identification, which may have far-reaching application potential in robotic taste, the food industry and in environmental sensing[25].

Furthermore, the TDTS is able to feed back an instantaneous response signal within 90 ms of a falling droplet (Fig. 4d), whether it is drinking water, sugar water or white vinegar with poor fluidity, indicating the sensitive detection capability of the sensor. Meanwhile, the output performance of the TDTS maintains a high detection stability even after 500 droplets are repeatedly dropped (Fig. 4e and Supplementary Fig. 10). In addition, long-term working tests (about 500 droplets) of the TDTS at different pH conditions and temperature and humidity stability tests are shown in Supplementary Figs. 11–17. In terms of the application environment, the TDTSs show high stability in the face of different conditions. Thus, we obtain a triboelectric taste sensor with a simple structure, low cost, stable performance, sensitive response and widespread application. The triboelectric fingerprint signal characteristics of different liquids can be extracted effectively to complete liquid identification in various application scenarios.

Deep-learning-enabled TDTS for liquid identification

Except for the shallow features (such as magnitude, time slot and total time) from the current waveform, the dual-triboelectric signals induced by droplets contain much subtle information that cannot be identified by the naked eye. As an emerging technology to extract subtle differences, deep learning has been applied to triboelectric signal analysis[14,26,27]. In particular, a convolutional neural network (CNN) can effectively extract small but important features hidden in the signals through its convolutional layers, becoming another effective tool in deep learning[28,29]. Thus, we propose an intelligent droplet-based triboelectric taste-sensing system. With the assistance of the image recognition technology based on the CNN, the system is expected to realize the robotic perception and identification of many common

https://doi.org/10.1038/s43016-023-00817-7

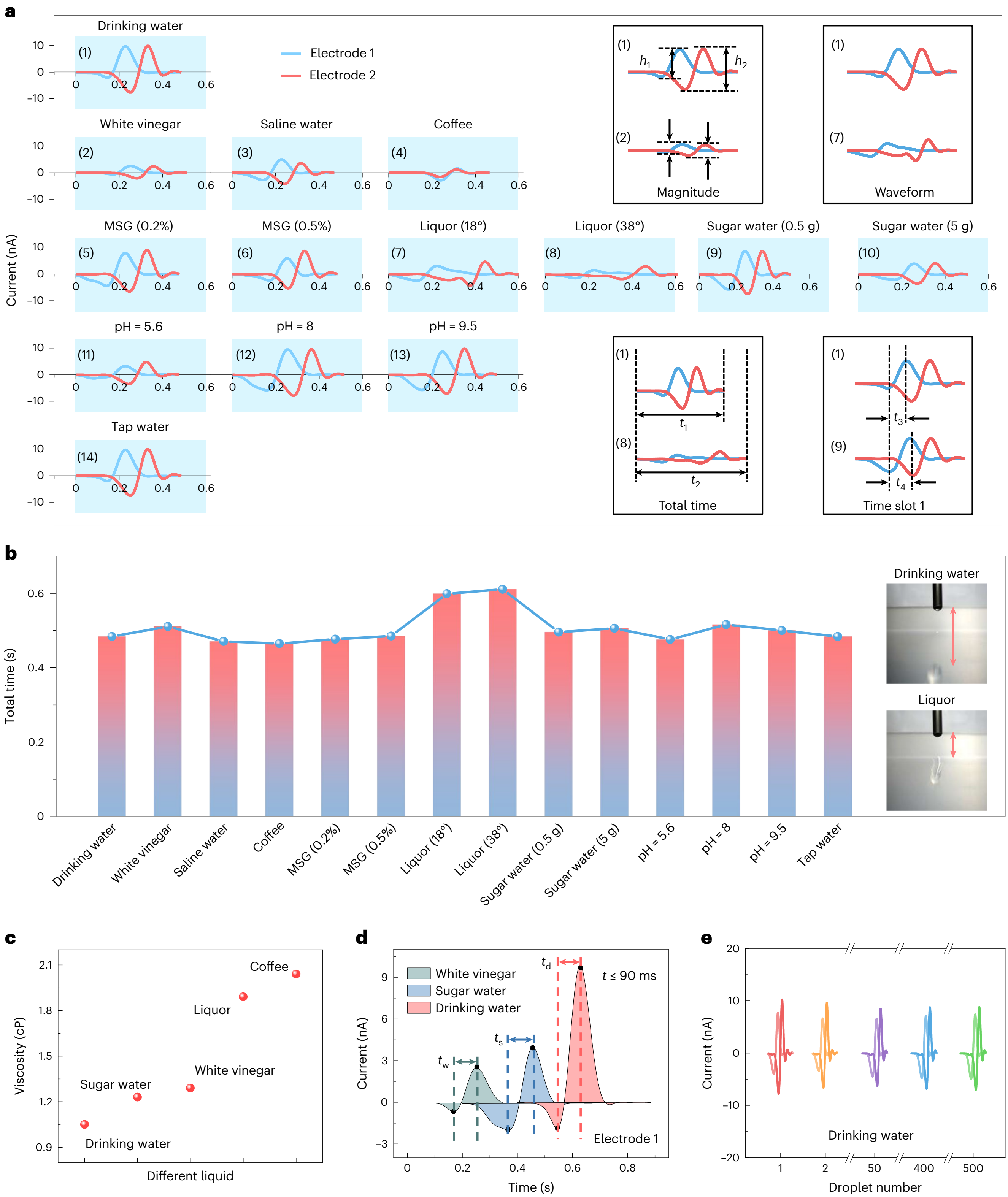

Fig. 4 | Feature extraction of different liquids from droplet-induced triboelectric signals. a, Liquid characteristics (including magnitude, waveform, full waveform time and valley-to-peak time slot corresponding to electrode 1) obtained from current signals when the TDTS identifies 14 liquids. t_1, total time required for drinking water to form a complete waveform; t_2, total time required for liquor (38°) to form a complete waveform; t_3, time slot of drinking water from the valley to the peak; t_4, time slot of sugar water (0.5 g) from the valley to the peak; t_w, response time of TDTS to white vinegar; t_s, response time of TDTS to sugar water; t_d, response time of TDTS to drinking water. **b**, Summary of the total time for a complete waveform for different identified liquids. The red arrows indicate the distance of liquids sliding in the same time, which can intuitively show that drinking water slides faster than liquor. **c**, Viscosity test of five liquids (drinking water, sugar water, white vinegar, liquor and coffee). **d**, Response time of the TDTS to three types of liquid. **e**, The current signal generation performance for the TDTS with hundreds of water droplets. The different colours represent signal curves at several moments in the current signals repeatedly contacted by the TDTS and 500 droplets.

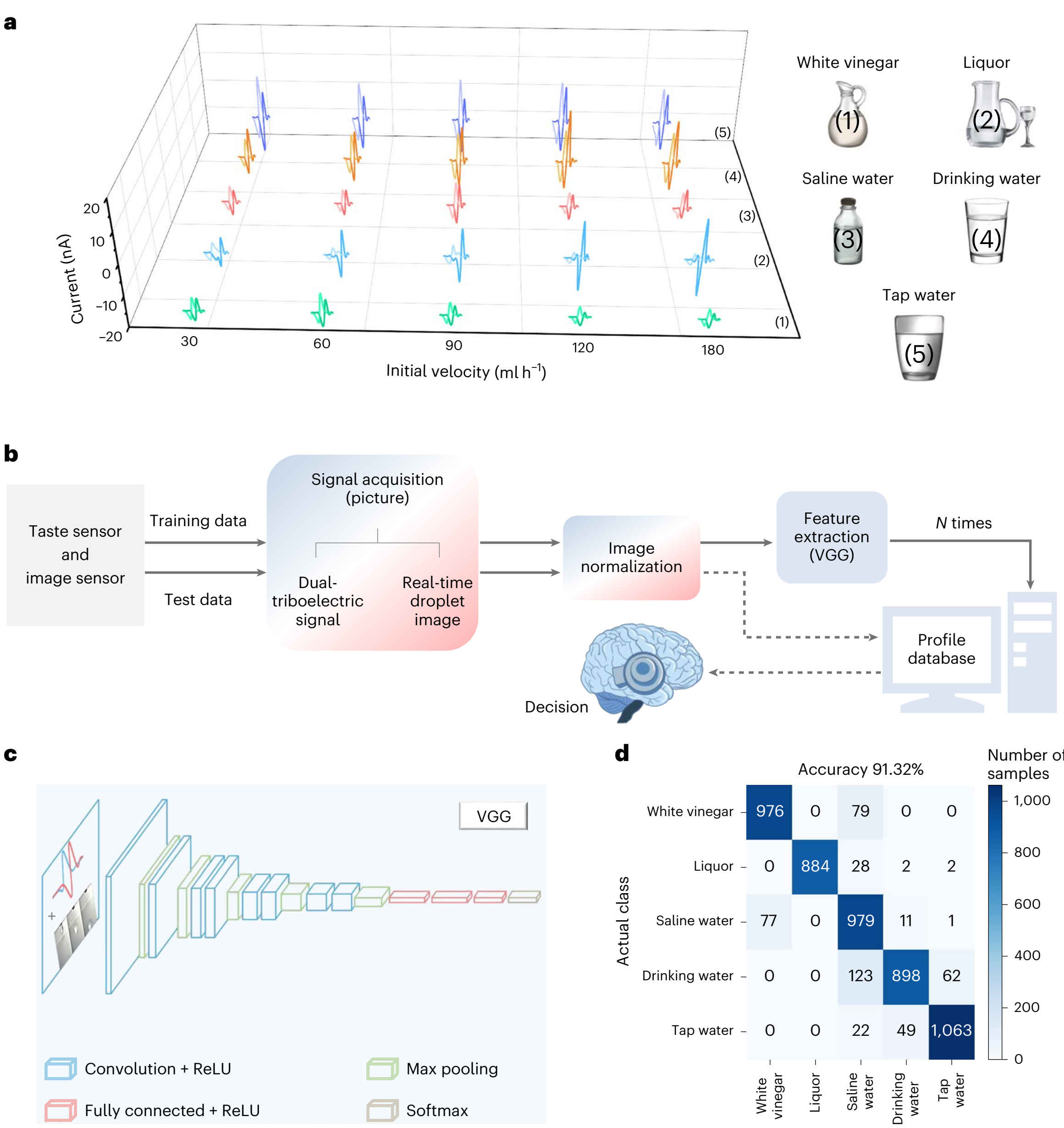

Fig. 5 | Deep-learning-based data processing for liquid-type identification. **a**, Dual-triboelectric signal acquisition provided for deep-learning training of robotic taste-related liquids. **b**, Flow diagram of training and test data based on deep learning for liquid recognition. **c**, The detailed structure of a neural network training model (VGG). **d**, Confusion map for the 5 different liquids, with an accuracy of 91.3%. There are 1,055 samples of white vinegar, of which 976 are predicted correctly and 79 are predicted incorrectly as saline water.

liquids, along with complex signal analysis and liquid recognition in several application scenarios.

For robotic taste sensing, multiple triboelectric signals from five real-life liquids are collected (white vinegar, liquor, saline water, drinking water and tap water; Fig. 5a). To accommodate various parameters in practical application scenarios and achieve higher accuracy of complex identification tasks, the collected raw signals include different initial velocities, falling angles and different liquids. Using the same method, the current signals of the associated droplets were also collected, including flavour analysis of liquid food (white vinegar, black coffee, saline water, drinking water and MSG solution; Supplementary Fig. 18), environmental monitoring (pH = 5.6, pH = 8, pH = 9.5, drinking water and tap water; Supplementary Fig. 19), and alcohol and sugar range tests (liquor with different alcoholicity, sugar water with different concentrations and drinking water; Supplementary Fig. 20). More concretely, the total dataset used for robotic taste sensing is from five different liquids, containing 52,586 samples (training set, 47,330; test set, 5,256). In addition, 43,501 samples were used for flavour analysis of liquid food (training set, 39,153; test set, 4,348); 42,528 samples were applied to environmental monitoring (training set, 38,277; test set, 4,251); 31,939 samples were used for the sugar test (training set, 28,746; test set, 3,193); and the training dataset contained 28,286 samples (training set, 25,459; test set, 2,827) for the alcohol range test.

Figure 5b shows the flow diagram of liquid recognition using the TDTS with the assistance of deep learning. Before model training, the collected droplet data (saved in the form of images) are normalized. After feature extraction, 90% of the data are used for Visual Geometry Group (VGG) model training, and the remaining data are used to test

https://doi.org/10.1038/s43016-023-00817-7

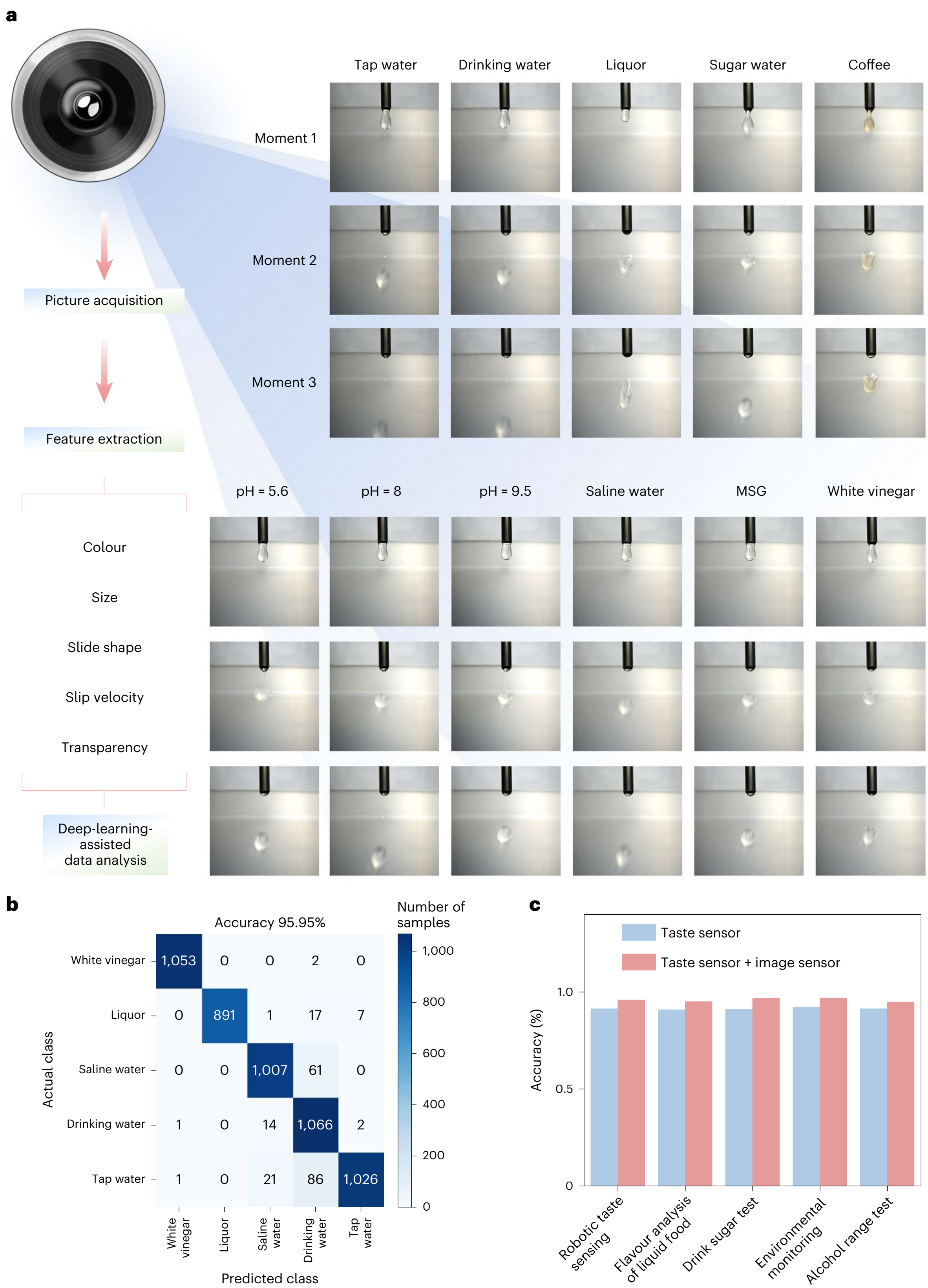

Fig. 6 | Synergistic effect of triboelectric signals and image features for a higher accuracy of liquid identification. a, Sliding process images of different liquids for deep-learning data analysis. **b**, Confusion matrix of five liquids using the intelligent droplet-based taste-sensing system containing the triboelectric taste sensor and the image sensor, with an accuracy of 96.0% for liquid recognition. There are 1,055 samples of white vinegar, of which 1,053 are predicted correctly and 2 are predicted incorrectly as drinking water. **c**, Comparison of sensing ability between the self-powered taste–vision liquid-sensing system (fusing a TDTS and an image sensor) and the TDTS.

https://doi.org/10.1038/s43016-023-00817-7

the accuracy of the model. Here the VGG model consists of eight convolutional and rectified linear unit (ReLU) layers, five pooling layers and three fully connected layers. The pre-processed data are colour images with uniform size (the input size is 261 × 381 × 3, where 261 and 381 pixels represent the height and width of the image, respectively, and 3 represents the number of channels). The network structure of the VGG model is shown in Fig. 5c. The liquid recognition accuracy rate reaches up to 91.3% under the premise of using only the taste-sensing system. The corresponding confusion matrix of the five liquids is shown in Fig. 5d.

Synergistic effect of triboelectric signal and image features

The complete characteristics of liquids also need to take into account their visual aspects. Both perceptual modes (taste and vision) can provide complementary information about liquids, which makes the analysis of liquids more comprehensive and meaningful[30]. In this work, we choose a commercial image sensor for single or continuous droplet image acquisition. Similar to the deep-learning-assisted data analysis process of the droplet-based taste-sensing system, the first step is image data acquisition. In the experiment, three images are acquired for each unknown droplet, and the images are taken from three moments when the droplet slides. Moment 1 is defined as the moment when the droplet is about to fall from the needle, moment 2 is regarded as the moment when the droplet just touches the FEP inclined plane, and the next moment after the droplet has touched the plane is moment 3. As shown in Fig. 6a, it is clear that the images presented by different droplets are quite different under the same sliding time, which is related to their morphology or physical properties. Black coffee has the most obvious colour characteristics, whereas liquor and white vinegar have a relatively slow sliding speed, which coincides with the total time of droplet sliding shown in Fig. 4b. Furthermore, the obvious deformation of liquor at moment 3 may be recognized as a typical feature of liquor, which also fully corresponds to the special waveform that occurs during the sliding process of liquor (Fig. 4a). Numerous effective features, including colour, size, slide shape, slip velocity and transparency, can be extracted for liquid identification. The subtle differences between these features and deeper features contribute to coping with complex recognition scenarios.

Inspired by the multimodal characterization of red wine[30], we consider realizing droplet-triggered liquid recognition in an integrated taste–vision sensing system. Relying on the synergistic effect of a TDTS and an image sensor, the features obtained from triboelectric sensing signals and visualized images are fused, and then associate with these two types of feature data through the VGG model. After training, this dual-sensory fusion liquid-sensing system can effectively enhance the sensing function of liquids, with an accuracy of 96.0% (Fig. 6b). We also analyse and compare the recognition accuracy of using only the taste sensor and using both the taste sensor and the image sensor (Supplementary Figs. 21–28). It is worth acknowledging that the accuracy of the recognition system using only the taste sensor is consistently higher than 90%, demonstrating its ability to recognize liquids. In addition, the cooperation of the image sensor further enhances the discriminating faculties. The experimental results show that the accuracy of the combined system is higher than that of using only the taste sensor (Fig. 6c). The results of this work also show that the discrimination capabilities of the intelligent taste-sensing system can be significantly improved when features from each liquid are combined to form multimodal features. The process of simulating taste perception for several different liquids is shown in detail in Supplementary Video 7.

Discussion

Inspired by the perceptual mechanisms of the human taste system, we propose an intelligent triboelectric taste-sensing system. When different droplets slide through the sensing electrodes, triboelectric signals with unique characteristics can be actively generated. These characteristic differences depend on a series of liquid-phase differences triggered by the liquid type, including droplet charge-transfer ability, ion concentration, pH value, liquid composition, viscosity and slip morphology. With the aid of deep learning, the feature information of five common liquids (white vinegar, liquor, saline water, drinking water and tap water) is identified. Under the premise of using only two independent electrodes, the recognition accuracy reaches 91.3%. This self-powered droplet-based triboelectric taste-sensing system provides a feasible strategy for developing effective and low-cost liquid-sensing technology. In addition, a complete liquid description is inseparable from the visual characteristics of liquids. Therefore, we present an intelligent dual-sensory self-powered liquid-sensing system that integrates the taste and visual information of different liquids. The introduction of visual features complements the liquid recognition function with an accuracy of 96.0%. To broaden the application, we used these two systems to detect the relevant liquids in five applications (robotic taste sensing, flavour analysis of liquid food, sugar detection, environmental monitoring and alcohol content test). The identification accuracy of both systems is higher than 90%, which sufficiently attests to the powerful perception of these two sensing systems. The integrated system is well ahead in recognition.

Future strategies will include developing sensing arrays with new materials and sensing systems with multisensor information fusion. In addition, sampling databases constructed with complete features, construction of flexible model frameworks of deep learning, and the development of a miniaturized, intelligent and multifunctional sensing system are needed. With the development of higher-level detection capabilities and the implementation of a wider identification space, this intelligent dual-sensory liquid-sensing system has the potential to become a promising tool in the rapid detection of liquid food.

Methods

Materials

Film materials of different kinds and thicknesses (30 µm polytetrafluoroethylene (PTFE), 30 µm FEP, 30 µm polyvinyl chloride, 30 µm polyimide (Kapton), 60 µm PTFE and 80 µm PTFE) were purchased to compare the electrical properties and hydrophobicity in contact with droplets. The DI water used in the experiment was produced from a laboratory ultrapure water instrument system (Direct-Pure UP-10; RephiLe Bioscience), and DI water was also used in the configuration of the solutions required in the experiment. Unless otherwise indicated, drinking water was obtained from Jingtian bottled water, and tap water was taken from domestic water. In addition, white vinegar (Haitian vinegar, 5°) and liquor (Redstarwine, 42% vol.) were used. Saline water, coffee suspension, 0.2% and 0.5% MSG, and sugar water were all prepared from edible salt, black coffee, gourmet powder and white granulated sugar with DI water, respectively. Weak acid and weak base solutions with a pH of 5.6, 8 and 9.5 were obtained by diluting buffer solutions.

Fabrication of the TDTS

Two 1-cm-wide copper electrodes, approximately 4 cm apart, were glued onto a smooth and clean poly(methyl methacrylate) (PMMA) substrate ($6 \times 12 \times 0.2$ cm^3). After introducing wires separately, a 30 µm FEP film was carefully attached onto the PMMA plate with adhered electrodes. The attached FEP film must cover all areas of the copper electrodes to avoid electrical interference and chemical corrosion of the copper by liquid.

Characterization and measurement

We obtained droplets of various volumes using stainless steel needles with different orifice diameters (Dongguan Assist Hand Electronic Tools); outer diameter: 8 gauge (4 mm), 10 gauge (3.5 mm), 16 gauge (1.64 mm) and 17 gauge (1.48 mm). A single-channel microsyringe pump (LD-P2020, LANDE; Hebei Wali Electronic Commerce) was used to control the initial velocity of the droplets. A large number of high-resolution droplet images were captured in real time via an industrial camera (MV-CA050; Hikrobot Technology). The viscosity of fluids was measured with a rotary viscometer (Brookfield DV-II Pro). Triboelectric signals from different droplets sliding across the surface of the taste sensor were collected through Keithley electrometers with a LabVIEW program. Two programmable electrometers (6514; Keithley) work simultaneously to measure the two current signals. These data were acquired, processed and saved as a picture.

VGG model training and optimization

The network structure of VGG11 consists of eight convolution and ReLU layers, five pooling layers and three fully connected layers. Using the Adam optimizer, the learning rate is set to 0.0001, the total number of epochs is 3 and the batch size is 24. The CNN model is developed in the Pytorch library and trained on a NVIDIA GeForce RTX 2080 Ti. We can divide the network structure of VGG11 into two parts: (1) the first part extracts features from the input image samples, which is composed of a convolutional layer, a ReLU layer and a pooling layer. The convolution processing of the model is divided into five phases. The first time, 1 convolution operation with 64 convolution kernels is implemented. The second time goes through 1 convolution with 128 convolutional kernels, and the third time performs 2 convolution processes with 256 convolutional kernels. The fourth and fifth times adopt two convolution processes of 512 convolutional kernels. The ReLU function is repeated for all operations after convolution processes, and is then followed by a max-pooling layer. (2) The second part classifies the samples based on the features extracted from the first part, which consists of a fully connected layer, a ReLU layer and a softmax layer[31]. All the data are flattened into a one-dimensional vector, and the corresponding prediction results are output by the softmax function after three fully connected layers. In addition, because of the widely used small convolution kernels, the VGG11 model generally requires fewer iterations in convergence during the training process, which speeds up the training speed.

Reporting summary

Further information on research design is available in the Nature Portfolio Reporting Summary linked to this article.

Data availability

All relevant data are included in the article, Supplementary Information and the source data files provided with this paper. All the other raw data are available from the corresponding authors on request.

Code availability

The code is available from the corresponding authors upon reasonable request.

References

1. Vlasov, Y., Legin, A., Rudnitskaya, A., Di Natale, C. & D'amico, A. Nonspecific sensor arrays ('electronic tongue') for chemical analysis of liquids (IUPAC Technical Report). *Pure Appl. Chem.* **77**, 1965–1983 (2005).
2. Gabrieli, G., Muszynski, M. & Ruch, P. W. A reconfigurable integrated electronic tongue and its use in accelerated analysis of juices and wines. In *2022 IEEE International Symposium on Olfaction and Electronic Nose (ISOEN)* 1–3 (IEEE, 2022).
3. Zhu, Y. W. et al. Exploring the relationships between perceived umami intensity, umami components and electronic tongue responses in food matrices. *Food Chem.* **368**, 130849 (2022).
4. Sochacki, G., Abdulali, A. & Iida, F. Mastication-enhanced taste-based classification of multi-ingredient dishes for robotic cooking. *Front. Robot. AI* **9**, 886074 (2022).
5. Rodríguez-Méndez, M. L. et al. Electronic noses and tongues in wine industry. *Front. Bioeng. Biotechnol.* **4**, 81 (2016).
6. Woertz, K., Tissen, C., Kleinebudde, P. & Breitkreutz, J. Taste sensing systems (electronic tongues) for pharmaceutical applications. *Int. J. Pharm.* **417**, 256–271 (2011).
7. Winquist, F. et al. An electronic tongue in the dairy industry. *Sensor. Actuat. B* **111-112**, 299–304 (2005).
8. Fan, F. R., Tang, W. & Wang, Z. L. Flexible nanogenerators for energy harvesting and self-powered electronics. *Adv. Mater.* **28**, 4283–4305 (2016).
9. Lee, M. et al. Self-powered environmental sensor system driven by nanogenerators. *Energy Environ. Sci.* **4**, 3359–3363 (2011).
10. Wang, X. D. et al. Self-powered high-resolution and pressure-sensitive triboelectric sensor matrix for real-time tactile mapping. *Adv. Mater.* **28**, 2896–2903 (2016).
11. Zhong, T. Y. et al. An artificial triboelectricity-brain-behavior closed loop for intelligent olfactory substitution. *Nano Energy* **63**, 103884 (2019).
12. Guo, H. Y. et al. A highly sensitive, self-powered triboelectric auditory sensor for social robotics and hearing aids. *Sci. Robot.* **3**, eaat2516 (2018).
13. Yoon, H. J. et al. Mechanoreceptor-inspired dynamic mechanical stimuli perception based on switchable ionic polarization. *Adv. Funct. Mater.* **31**, 2100649 (2021).
14. Qu, X. C. et al. Artificial tactile perception smart finger for material identification based on triboelectric sensing. *Sci. Adv.* **8**, eabq2521 (2022).
15. Wei, X. L., Wang, B. C., Wu, Z. Y. & Wang, Z. L. An open-environment tactile sensing system: toward simple and efficient material identification. *Adv. Mater.* **34**, 2203073 (2022).
16. Bachmanov, A. A. & Beauchamp, G. K. Taste receptor genes. *Annu. Rev. Nutr.* **27**, 389–414 (2007).
17. Barretto, R. P. J. et al. The neural representation of taste quality at the periphery. *Nature* **517**, 373–376 (2015).
18. Kwak, S. S. et al. Triboelectrification-induced large electric power generation from a single moving droplet on graphene/polytetrafluoroethylene. *ACS Nano* **10**, 7297–7302 (2016).
19. Choi, M., Lee, W. M. & Yun, S. H. Intravital microscopic interrogation of peripheral taste sensation. *Sci. Rep.* **5**, 8661 (2015).
20. Wei, X. L. et al. All-weather droplet-based triboelectric nanogenerator for wave energy harvesting. *ACS Nano* **15**, 13200–13208 (2021).
21. Zhao, X. J., Zhu, G., Fan, Y. J., Li, H. Y. & Wang, Z. L. Triboelectric charging at the nanostructured solid/liquid interface for area-scalable wave energy conversion and its use in corrosion protection. *ACS Nano* **9**, 7671–7677 (2015).
22. Pan, L. et al. Liquid-FEP-based U-tube triboelectric nanogenerator for harvesting water-wave energy. *Nano Res.* **11**, 4062–4073 (2018).
23. Nie, J. H. et al. Probing contact-electrification-induced electron and ion transfers at a liquid-solid interface. *Adv. Mater.* **32**, 1905696 (2020).
24. Lin, S. Q., Xu, L., Chi Wang, A. & Wang, Z. L. Quantifying electron-transfer in liquid-solid contact electrification and the formation of electric double-layer. *Nat. Commun.* **11**, 399 (2020).
25. Ying, Z. H. et al. Self-powered liquid chemical sensors based on solid-liquid contact electrification. *Analyst* **146**, 1656–1662 (2021).
26. Shi, Q. F. et al. Deep learning enabled smart mats as a scalable floor monitoring system. *Nat. Commun.* **11**, 4609 (2020).
27. Wen, F. et al. Machine learning glove using self-powered conductive superhydrophobic triboelectric textile for gesture recognition in VR/AR applications. *Adv. Sci.* **7**, 2000261 (2020).
28. Shi, Q. F. et al. Artificial intelligence of things (AIoT) enabled floor monitoring system for smart home applications. *ACS Nano* **15**, 18312–18326 (2021).
29. Sundaram, S. et al. Learning the signatures of the human grasp using a scalable tactile glove. *Nature* **569**, 698–702 (2019).
30. Rodriguez-Mendez, M. L. et al. Fusion of three sensory modalities for the multimodal characterization of red wines. *IEEE Sens. J.* **4**, 348–354 (2004).

https://doi.org/10.1038/s43016-023-00817-7

31. Simonyan, K. & Zisserman, A. Very deep convolutional networks for large-scale image recognition. Preprint at https://arxiv.org/abs/1409.1556 (2014).

Acknowledgements

This research was supported by the National Natural Science Foundation of China (grant number 61503051; Z.W.).

Author contributions

Z.W. and Z.L.W. planned the study and supervised the whole project. X.W., Z.W. and Z.L.W. conceived the idea, analysed the data and wrote the paper. B.W., X.C. and H.Z. helped with the experiments. All the authors discussed the results and commented on the paper.

Competing interests

The authors declare no competing interests.

Additional information

Supplementary information The online version contains supplementary material available at https://doi.org/10.1038/s43016-023-00817-7.

Correspondence and requests for materials should be addressed to Zhiyi Wu or Zhong Lin Wang.

Peer review information *Nature Food* thanks Zong-Hong Lin and the other, anonymous, reviewer(s) for their contribution to the peer review of this work.

nature portfolio

Corresponding author(s): Zhong Lin Wang

Last updated by author(s): Apr 19, 2023

Reporting Summary

Nature Portfolio wishes to improve the reproducibility of the work that we publish. This form provides structure for consistency and transparency in reporting. For further information on Nature Portfolio policies, see our Editorial Policies and the Editorial Policy Checklist.

Statistics

For all statistical analyses, confirm that the following items are present in the figure legend, table legend, main text, or Methods section.

n/a	Confirmed	
☐	☒	The exact sample size (n) for each experimental group/condition, given as a discrete number and unit of measurement
☐	☒	A statement on whether measurements were taken from distinct samples or whether the same sample was measured repeatedly
☒	☐	The statistical test(s) used AND whether they are one- or two-sided *Only common tests should be described solely by name; describe more complex techniques in the Methods section.*
☒	☐	A description of all covariates tested
☒	☐	A description of any assumptions or corrections, such as tests of normality and adjustment for multiple comparisons
☒	☐	A full description of the statistical parameters including central tendency (e.g. means) or other basic estimates (e.g. regression coefficient) AND variation (e.g. standard deviation) or associated estimates of uncertainty (e.g. confidence intervals)
☒	☐	For null hypothesis testing, the test statistic (e.g. F, t, r) with confidence intervals, effect sizes, degrees of freedom and P value noted *Give P values as exact values whenever suitable.*
☒	☐	For Bayesian analysis, information on the choice of priors and Markov chain Monte Carlo settings
☒	☐	For hierarchical and complex designs, identification of the appropriate level for tests and full reporting of outcomes
☒	☐	Estimates of effect sizes (e.g. Cohen's d, Pearson's r), indicating how they were calculated

Our web collection on statistics for biologists contains articles on many of the points above.

Software and code

Policy information about availability of computer code

Data collection	No software was used.
Data analysis	No software was used.

For manuscripts utilizing custom algorithms or software that are central to the research but not yet described in published literature, software must be made available to editors and reviewers. We strongly encourage code deposition in a community repository (e.g. GitHub). See the Nature Portfolio guidelines for submitting code & software for further information.

Data

Policy information about availability of data

All manuscripts must include a data availability statement. This statement should provide the following information, where applicable:

- Accession codes, unique identifiers, or web links for publicly available datasets
- A description of any restrictions on data availability
- For clinical datasets or third party data, please ensure that the statement adheres to our policy

All relevant data are included in the article, Supplementary Information and in the Source Data files provided with this paper. All the other raw data are available from the authors on request.

Research involving human participants, their data, or biological material

Policy information about studies with human participants or human data. See also policy information about sex, gender (identity/presentation), and sexual orientation and race, ethnicity and racism.

Reporting on sex and gender	n/a
Reporting on race, ethnicity, or other socially relevant groupings	n/a
Population characteristics	n/a
Recruitment	n/a
Ethics oversight	n/a

Note that full information on the approval of the study protocol must also be provided in the manuscript.

Field-specific reporting

Please select the one below that is the best fit for your research. If you are not sure, read the appropriate sections before making your selection.

☐ Life sciences ☐ Behavioural & social sciences ☒ Ecological, evolutionary & environmental sciences

For a reference copy of the document with all sections, see nature.com/documents/nr-reporting-summary-flat.pdf

Ecological, evolutionary & environmental sciences study design

All studies must disclose on these points even when the disclosure is negative.

Study description	This study presents an intelligent dual-sensory liquid sensing system and outputs a series of triboelectric signals that depend on the liquid properties. Combined with deep learning technology, a "liquid fingerprint database" can be established to implement the preliminary identification of different liquids, and a high accuracy of 91.3% is achieved in the robot taste application. Furthermore, the visual information of different droplets is fused to further extract the complete visual characteristics of liquids. Thus, a more comprehensive liquid recognition function can be achieved with the assistance of image recognition. The inclusion of liquid visual information further facilitates the perception capability of the taste sensing system, and the recognition accuracy is up to 96.0%. This dual-sensory fusion self-powered liquid sensing system, along with the sensing principle and design of the triboelectric droplet-tasting sensor, not only helps robots to perceive the external world, but also provides an effective and low-cost way of thinking for liquid food flavor, sugar detection, environmental monitoring, and alcohol content test, without any external power supply. It can be predicted that this intelligent liquid sensing system will serve as an effective mean of the liquid food safety rapid determination, which can improve the efficiency of food monitoring, expand the scope of food control, and has the initiative significance and motive effect for the food safety management system.
Research sample	The total dataset used for robotic taste sensing is from five different liquids (white vinegar, liquor, saline water, drinking water, and tap water), containing 52,586 samples; In addition, 43,501 samples were used for flavor analysis of liquid food (white vinegar, black coffee, saline water, drinking water, and MSG solution); 42,528 samples were applied to environmental monitoring (pH = 5.6, pH = 8, pH = 9.5, drinking water, and tap water); 31,939 samples were used for the drink sugar test; And the training dataset contained 28,286 samples for the alcohol range test (liquor with different alcoholicity, sugar water with different concentrations, and drinking water).
Sampling strategy	The selection of sample size mainly refers to previous related works. Of course, different sample and different sample sizes were selected for pre-experiments before determining the sample size, which can verify the uniformity of samples and reduce the influence of accidental samples on the experimental results. In addition, the random sampling method was applied to avoid the interference of subjectivity to the accuracy of the experiment .
Data collection	The data were collected through Keithley electrometers with a LabVIEW program. Two programmable electrometers (Keithley 6514) work simultaneously to measure the two current signals.
Timing and spatial scale	June 2nd-July 12th. The random sampling method was applied to avoid the interference of subjectivity to the accuracy of the experiment.
Data exclusions	No data were excluded from the analyses.
Reproducibility	All attempts to repeat the experiment were successful.
Randomization	n/a
Blinding	n/a

Did the study involve field work? ☐ Yes ☒ No

Reporting for specific materials, systems and methods

We require information from authors about some types of materials, experimental systems and methods used in many studies. Here, indicate whether each material, system or method listed is relevant to your study. If you are not sure if a list item applies to your research, read the appropriate section before selecting a response.

Materials & experimental systems

n/a	Involved in the study	
☒	☐	Antibodies
☒	☐	Eukaryotic cell lines
☒	☐	Palaeontology and archaeology
☒	☐	Animals and other organisms
☒	☐	Clinical data
☒	☐	Dual use research of concern
☒	☐	Plants

Methods

n/a	Involved in the study	
☒	☐	ChIP-seq
☒	☐	Flow cytometry
☒	☐	MRI-based neuroimaging